Phase Noise Suppression in MIMO LoS Systems for High Capacity Backhauling

Luca Reggiani · Gaudenzio Filiberti · Laura Dossi

Published online: 30 January 2015

1 Introduction

The rapidly evolving scenario of cellular communications is driving the change of requirements for the underlying telecommunication infrastructure, so facing the problem of guaranteeing very high throughput backhauling connectivity. If a cost-effective solution is the

L. Reggiani
DEIB, Politecnico di Milano, Milan, Italy
e-mail: luca.reggiani@polimi.it

G. Filiberti
Via C. Battisti, 112, Invorio, NO, Italy
e-mail: gaudenzio.filiberti@alice.it

L. Dossi (✉)
IEIIT CNR, c/o DEIB, Politecnico di Milano, Milan, Italy
e-mail: laura.dossi@ieiit.cnr.it

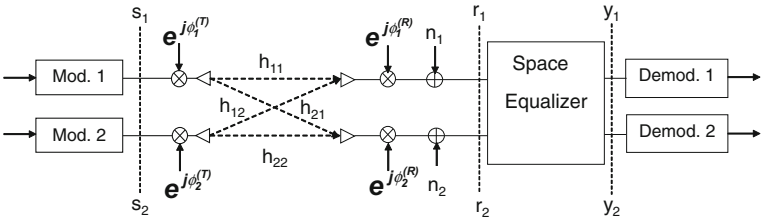

Fig. 1 System model and receiver architecture. The effects of electronic impairments are modeled as additive (thermal noise) sources, named as n_i, and multiplicative (phase noise) sources, named as $e^{\phi_i^{(T)}}$ and $e^{\phi_i^{(R)}}$, with $i = 1, 2$. The index k representing the discrete time instant is not reported for the sake of clarity

point-to-point (PtP) microwave link in conventional radio frequency (RF) licensed bands (from 15 to 42 GHz, typically 18, 23, 38, and 42 GHz) and in the new E-band (74 and 84 GHz) [1–3], on the other hand these microwave radio links risk to become the bottle-neck in the deployment of future cellular networks due to the huge increase of mobile data traffic. This bottleneck can be overcome by exploiting spatial multiplexing, obtained by a careful placement of antennas at transmitter and receiver; this is the idea behind LoS-MIMO system [4–6]. A LoS-MIMO (2×2) connection equipped with a smart, expanded form of adaptivity for embracing the extreme configurations of MIMO arrangement, has been proved to satisfy the stringent requirements in terms of outage and reliability while achieving the capacity increase requested by next generation backhauling networks [7]. In [7] the authors highlighted how in practical design of LoS-MIMO systems the phase noise impact increases at low antenna separations becoming dominant w.r.t. the other impairment sources.

In the literature, the impact and suppression of phase noise in MIMO systems have been investigated theoretically in many papers, especially for finding MIMO capacity in presence of Wiener phase noise [8]. For a rich literature survey the reader can refer to [8].

In this work our aim is to give some design lines in the practical implementation of a LoS-MIMO (2×2) system as presented in Sect. 2 and the novel contributions can be summarized as follows:

- Three different architectures for phase noise suppression are presented and analyzed for revealing performance and implementation differences (Sect. 3).
- The comparison between simple linear interpolators and Wiener filters in the pilot assisted phase estimation process is discussed for revealing possible system simplifications in the LoS-MIMO case (Sect. 3 and 5).
- The impact of the use of coherent oscillators at receiver or transmitter on the output phase noise and its effect on the overall system performance is investigated (Sect. 4 and 5). In the sequel, Sect. 2 presents the system model and Sect. 3 describes the methods and the architectures used for phase noise estimation and suppression in the context of this application. Then Sect. 4 is devoted to the analytical derivations of the phase noise impact on the system performance under different design choices and, finally, in Sect. 5, the numerical results are presented and commented.

2 System Model

The system model of the LoS-MIMO (2×2) is sketched in Fig. 1. Thermal and phase noises are modeled as an additive processes at the receiver, named as n_i, and as multiplicative

processes $e^{j\phi_i^{(T)}}$ and $e^{j\phi_i^{(R)}}$ respectively at transmitter and receiver, with $i = 1, 2$. The received signal at a certain instant k can be expressed in matrix form as

$$\mathbf{r}_k = \boldsymbol{J}_{Rx;k}\boldsymbol{H}_k\boldsymbol{J}_{Tx;k}\mathbf{s}_k + \mathbf{n}_k, \tag{1}$$

with

$$\mathbf{s}_k = \begin{bmatrix} s_{1;k} & s_{2;k} \end{bmatrix}^T, \tag{2}$$

$$\mathbf{r}_k = \begin{bmatrix} r_{1;k} & r_{2;k} \end{bmatrix}^T, \tag{3}$$

$$\mathbf{n}_k = \begin{bmatrix} n_{1;k} & n_{2;k} \end{bmatrix}^T, \tag{4}$$

$$\boldsymbol{J}_{Rx;k} = \begin{bmatrix} e^{j\phi_{1;k}^{(R)}} & 0 \\ 0 & e^{j\phi_{2;k}^{(R)}} \end{bmatrix}, \tag{5}$$

$$\boldsymbol{J}_{Tx;k} = \begin{bmatrix} e^{j\phi_{1;k}^{(T)}} & 0 \\ 0 & e^{j\phi_{2;k}^{(T)}} \end{bmatrix}, \tag{6}$$

and the LoS-MIMO channel, here assumed deterministic, is given by

$$\boldsymbol{H}_k = \boldsymbol{H} = \begin{bmatrix} h_{11} & h_{12} \\ h_{21} & h_{22} \end{bmatrix} = G \cdot \begin{bmatrix} 1 & e^{-j\phi_0} \\ e^{-j\phi_0} & 1 \end{bmatrix}, \tag{7}$$

where G is a complex gain, including channel gain, antenna gains and phase rotation of the direct paths, and ϕ_0 [°] is the electrical phase difference between the direct and the cross paths. Without loss of generality, G will be assumed equal to 1 and the angle ϕ_0 is easily found as a function of the link distance R [m], antenna separation d [m] and wavelength λ [m], for $d << R$, as [7]

$$\phi_0 \approx 360\frac{d^2}{2R\lambda}. \tag{8}$$

At the receiver the space equalizer block combines linearly the two received signals for canceling their mutual interference. We remind that space equalization at high Signal-to-Noise Ratio (SNR) values (i.e. the usual working condition for high capacity LoS fixed links) is performed in a zero-forcing (ZF) form, inverting the MIMO channel matrix as

$$\boldsymbol{W} = (\boldsymbol{H}^*\boldsymbol{H})^{-1}\boldsymbol{H}^* = \frac{1}{1 - e^{-j2\phi_0}} \begin{bmatrix} 1 & -e^{-j\phi_0} \\ -e^{-j\phi_0} & 1 \end{bmatrix} \tag{9}$$

and operating as a co-polar interference canceler (CPIC) for the recovered signals y_i ($i = 1, 2$).

The four phase noise processes $\phi_n^{(T)}$ and $\phi_m^{(R)}$ (in the sequel $m = 1, 2$ is the receiver index while $n = 1, 2$ the transmitter one) represent the short-term random phase fluctuations, ignoring oscillator frequency drift. They are assumed zero mean and with total power ε_{TOT}^2. They are modeled by specifying a classical oscillator phase-noise power spectral density profile, with the definition of three basic frequency regions. A high frequency region that shows a nearly flat response called noise floor (the phase noise is mainly determined by the active device thermal noise), an intermediate frequency region where phase noise typically increases with a 20 dB per decade rate, and a last, low frequency region where the flicker noise dominates and the phase noise increases till to 30 dB per decade. In our simulations, the value of the noise power spectral density w.r.t. the carrier power (in dBc/Hz) is defined

at the different frequency offsets [10, 100, 1,000] kHz; once fixed this model, a particular phase noise process will be referred through its power density value at 100 kHz or its total power ε^2_{TOT}. In addition, in order to consider architectures in which the oscillator sources at the transmitter and at the receiver can be shared by the two branches, we introduce also two correlation factors, ρ_T and ρ_R, which reproduce the correlation degree between the two phase noise processes at the transmitter and at the receiver respectively. We will see that this aspect has a non negligible impact on the final system performance; in particular we will consider the two extreme cases, i.e. independent phase noise processes ($\rho_T = 0$ or $\rho_R = 0$, namely independent local oscillators) or coincident phase noise processes ($\rho_T = 1$ or $\rho_R = 1$), namely one single local oscillator at the transmitter or at the receiver.

3 Phase Noise Estimation and Suppression

Two steps are necessary for achieving an efficacious suppression of the phase noise: estimation of the phase noise samples and cancelation from the signal streams. Both steps, straightforward in the single antenna case, have non trivial aspects and implications in the MIMO system since in the received signals, each one a superposition of the two transmitted streams, the original phase noise processes are summed in different ways giving rise to (2×2) processes to be estimated. So we have two main differences in the MIMO systems w.r.t. Single Input Single Output (SISO) ones: (I) the phase noise estimation involves all the (2×2) linear combinations of the phase noise sources, and (II) phase noise cancelation is not performed in a single step, but more phase rotations have to be operated before, after or integrated into the space equalization block. Referring to the phase noise estimation methods, we may distinguish between solutions based on

- digital phase locked loop (DPLL) circuits, which track phase variations in the received signals by means of feedback mechanisms;
- non data aided (NDA) algorithms, which remove the data dependency on the received signals to recover the phase variations by operations like, for example, raising at the M-power;
- decision directed (DD) algorithms, which estimate phase variations by exploiting previous detected symbols;
- pilot aided (PA) algorithms, where periodic patterns of known symbols are exploited for recovering the phase variations at the corresponding locations and then phase estimation in the other symbol positions are operated by means of appropriate filtering (in this case we refer to them as *linear* PA algorithms).

In general NDA algorithms suffer from lower performance than other techniques and, in addition, their application is limited by particular modulations (e.g. M-PSK). DD techniques are limited by error propagation and latency while DPLL are typically limited by their bandwidth, which means a limited tracking ability of phase noise processes. For a MIMO system, which suffers from the impact of phase noise more than the corresponding SISO system [7] and needs high quality signal output for supporting high data rates, the PA solution is considered here the appropriate design choice, as observed also by other authors [9].

In Sect. 3.1 we resume the main PA phase noise estimation techniques while Sect. 3.2 is dedicated to the different cancelation or suppression architectures of practical interest for our application.

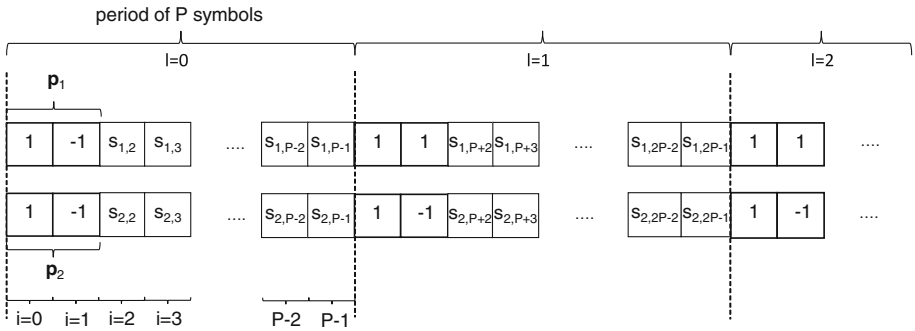

Fig. 2 Periodic pilot pattern for LoS-MIMO (2×2)

3.1 Linear Pilot Based Estimators

The PA estimation procedure consists of two steps, i.e. (I) the estimate of the phase noise samples at the pilots locations and (II) the linear filtering of the estimated samples to obtain the intra-period phase noise values. In the LoS-MIMO (2×2) system, we assume a periodic pilot pattern of P symbols characterized by a couple of adjacent pilots and $(P-2)$ consecutive data symbols. The two streams (each one transmitted from one antenna) have orthogonal couples of pilots, so allowing the recovery of all the four phase sum-processes from the two received signals (Fig. 2). The $(P-2)$ intra-period phase noise samples estimators are mostly based on the following techniques:

1. Wiener's filter, i.e. the well known minimum mean squared error (MMSE) solution to the estimation problem and whose details for MIMO systems can be found in [9].
2. Interpolation filters, which estimate the $(P-2)$ intra-period phase samples by interpolat-ing a set of adjacent pilots phases. Here we consider only the linear case, corresponding to the first order interpolator, which exploits only the two pilots phases immediately before and after the phase noise sample to be estimated.

The four sum-processes are defined and estimated at the pilots locations [9]:

$$\begin{aligned}
\varphi_{11;k} &= \phi_{1;k}^{(T)} + \phi_{1;k}^{(R)}, \\
\varphi_{21;k} &= \phi_{1;k}^{(T)} + \phi_{2;k}^{(R)}, \\
\varphi_{12;k} &= \phi_{2;k}^{(T)} + \phi_{1;k}^{(R)}, \\
\varphi_{22;k} &= \phi_{2;k}^{(T)} + \phi_{2;k}^{(R)}.
\end{aligned} \tag{10}$$

So the received signals $r_{m;k}$ with $m = 1, 2$,

$$\begin{aligned}
r_{1;k} &= e^{j\varphi_{11;k}} h_{11;k} s_{1;k} + e^{j\varphi_{12;k}} h_{12;k} s_{2;k} + n_{1;k}, \\
r_{2;k} &= e^{j\varphi_{21;k}} h_{21;k} s_{1;k} + e^{j\varphi_{22;k}} h_{22;k} s_{2;k} + n_{2;k},
\end{aligned} \tag{11}$$

at a generic couple of consecutive pilot locations, i.e. for $k = lP$ and $k = lP + 1$ with the index l spanning over the entire sequence of symbol periods, are multiplied each one by the two orthogonal couple of pilots $\mathbf{p}_1 = [1, 1]^T$ and $\mathbf{p}_2 = [1, -1]^T$ (Fig. 2) (it is assumed that phase noise samples do not change significantly over two consecutive symbols) and the channel phase ϕ_0, supposed known, is added to obtain the four real variables

$$
\begin{aligned}
\eta_{11;lP+1} &= arg\left([r_{1;lP}, r_{1;lP+1}] \cdot \mathbf{p}_1^*\right) \approx \varphi_{11;lP+1} + \widetilde{n}_{11;lP+1},\\
\eta_{21;lP+1} &= arg\left([r_{2;lP}, r_{2;lP+1}] \cdot \mathbf{p}_1^*\right) + \phi_0 \approx \varphi_{21;lP+1} + \widetilde{n}_{21;lP+1},\\
\eta_{12;lP+1} &= arg\left([r_{1;lP}, r_{1;lP+1}] \cdot \mathbf{p}_2^*\right) + \phi_0 \approx \varphi_{12;lP+1} + \widetilde{n}_{12;lP+1},\\
\eta_{22;lP+1} &= arg\left([r_{2;lP}, r_{2;lP+1}] \cdot \mathbf{p}_2^*\right) \approx \varphi_{22;lP+1} + \widetilde{n}_{22;lP+1}.
\end{aligned} \tag{12}
$$

Noise processes $\widetilde{n}$ are uncorrelated due to orthogonality of pilot sets.

In the Wiener filter case, variables (12) are observed during F pilot periods ($F \cdot P$ symbols), and $(F+1)$ observables are collected in a vector denoted as $\boldsymbol{\eta}_{lP}$. To estimate the phase noise processes $\widehat{\varphi}_{mn;lP+i}$, where $i = 2, \ldots, P-1$ is the interpolating symbol instant inside the l-th period, four vectors of filter coefficients $\mathbf{w}_{mn;i}$ of length $(F+1)$ are computed ($m = 1, 2$ and $n = 1, 2$). Details of this Wiener filter [9–11] applied to the LoS-MIMO (2×2) system are given in Appendix Sect. 7. The final phase estimation errors are defined as $\varphi^e_{mn;lP+i} = (\widehat{\varphi}_{mn;lP+i} - \varphi_{mn;lP+i})$. In the analysis, they are assumed uncorrelated, independent from the correlation degree of the oscillators, and identically distributed w.r.t. the period l and the indexes (m, n), i.e. $E[(\varphi^e_{mn;lP+i})^2] = \epsilon^2$.[1]

Finally, in the first order linear interpolator the observation vector is limited to the pilots just before and after each location inside a generic period (i.e. $F = 1$) and the filter coefficients are simply given by

$$
\mathbf{w}_{mn;i} = \begin{bmatrix} w_{11;i;1} \\ w_{11;i;2} \\ \hline w_{21;i;1} \\ w_{21;i;2} \\ \hline w_{12;i;1} \\ w_{12;i;2} \\ \hline w_{22;i;1} \\ w_{22;i;2} \end{bmatrix} = \begin{bmatrix} 1 - i/P \\ i/P \\ \hline 1 - i/P \\ i/P \\ \hline 1 - i/P \\ i/P \\ \hline 1 - i/P \\ i/P \end{bmatrix}. \tag{13}
$$

In accordance to the MMSE principle, the linear interpolator coefficients $\mathbf{w}_{mn;i}$ can be modified further by a multiplicative factor $w = 1 + (\sigma_n^2/E_S)/(2\varepsilon^2_{TOT})$ for moderating their impact w.r.t. the dominant contribution on the carrier phase between thermal and phase noises.

3.2 Architectures for Phase Noise Suppression

As anticipated in Sect. 3.1, once the four angles $\varphi_{mn;k}$ are estimated in a generic period between pilots, for $k = lP + 2, \ldots, lP + P - 1$, their cancelation must be integrated in the space equalization process, which separates the two transmitted data streams overlapped at the receiver by means of a combination of the estimated angles $\widehat{\varphi}_{mn;k}$. In fact, it is easy to realize that it is not possible to correct directly the four angles $\varphi_{mn;k}$ in a single step before the equalization, but two phase correction steps have to be introduced in the receiver in order to recover the transmitted symbols $s_{n;k}$.

In the LoS-MIMO (2×2) system we have selected three receiver structures that implement phase noise cancelation and space equalization, characterized by different architectural choices and presenting different implementation and performance pros and cons:

[1] Notice the difference between ε^2_{TOT}, i.e. the sources phase noise power and ϵ^2, i.e. the residual phase noise power after phase noise estimation.

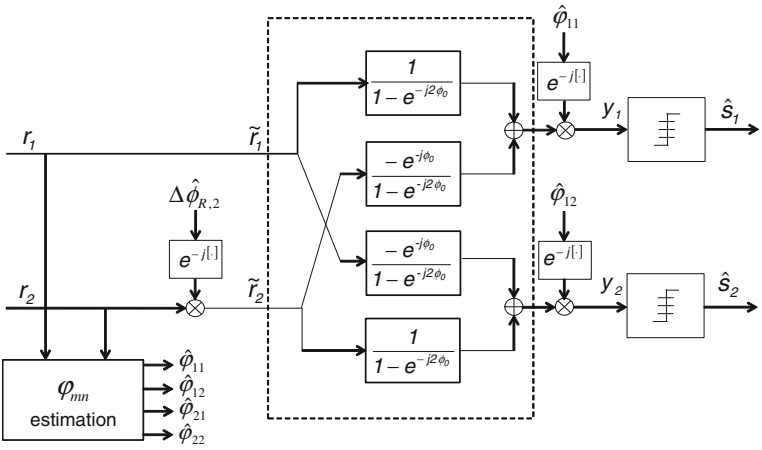

Fig. 3 Block diagram of asymmetric receiver with $\Delta\phi_R$ correction

1. Asymmetric receiver with $\Delta\phi_R$ correction.
2. Symmetric receiver with $\Delta\phi_R$ correction.
3. Symmetric receiver with $\Delta\phi_T$ correction.

The angles $\Delta\phi_R = \phi_2^{(R)} - \phi_1^{(R)}$ and $\Delta\phi_T = \phi_2^{(T)} - \phi_1^{(T)}$ are here defined as the phase noise difference at the receiver side and at the transmitter side respectively (for the sake of clarity we omit the samples index k).

3.2.1 Asymmetric Receiver with $\Delta\phi_R$ Correction

A receiver structure implementing phase noise cancelation and space equalization is described in the block diagram of Fig. 3. In the scheme, three stages can be observed:

- The phase rotation of the signal received on the second antenna r_2 by $(-\Delta\widehat{\phi}_{R2})$ computed as

$$\Delta\widehat{\phi}_{R2} = \widehat{\varphi}_{22} - \widehat{\varphi}_{12} = (\varphi_{22} - \varphi_{12}) + (\varphi^e_{22} - \varphi^e_{12}) = \Delta\phi_R + \Delta\phi^e_{R2}, \tag{14}$$

  sum of $\Delta\phi_R$ and the estimation error term $\Delta\phi^e_{R2} = (\varphi^e_{22} - \varphi^e_{12})$ where the subscript indicates that it depends also on the phase noise generated at transmitter 2 (10).
- The space equalization performed according to (9), where ϕ_0 is assumed perfectly known. In fact it is easy to realize that the signal $\mathbf{r}$, after the phase correction block,

$$\widetilde{\mathbf{r}} = \begin{bmatrix} e^{j\varphi_{11}} & e^{j(-\phi_0+\varphi_{12})} \\ e^{j(-\phi_0+\varphi_{21}-\Delta\widehat{\phi}_{R2})} & e^{-j\Delta\widehat{\phi}_{R2}} \end{bmatrix} \cdot \begin{bmatrix} s_1 \\ s_2 \end{bmatrix} + \begin{bmatrix} n_1 \\ n_2 e^{-j\Delta\widehat{\phi}_{R2}} \end{bmatrix}, \tag{15}$$

  in absence of additive noise and phase estimation errors is equal to $\mathbf{H} \cdot [\widetilde{s}_1, \widetilde{s}_2]^T$ with $\widetilde{s}_1 = s_1 e^{j\varphi_{11}}$ and $\widetilde{s}_2 = s_2 e^{j\varphi_{12}}$.
- The direct phase noise cancelation on the two branches by respectively $\widehat{\varphi}_{11}$ and $\widehat{\varphi}_{12}$ as a direct consequence of the previous step.

At the output of the receiver the resulting symbols y_1 and y_2 can be expressed explicitly as functions of the transmitted symbols and of the estimated phase noises as

$$\begin{aligned}
y_1 = & \frac{1}{1-e^{-j2\phi_0}}\Big[s_1\left(e^{\,j(\varphi_{11}-\widehat{\varphi}_{11})}-e^{\,j(-2\phi_0+\varphi_{21}-\widehat{\varphi}_{22}+\widehat{\varphi}_{12}-\widehat{\varphi}_{11})}\right)\\
& +s_2\left(e^{\,j(-\phi_0+\varphi_{12}-\widehat{\varphi}_{11})}-e^{j(\varphi_{22}-\widehat{\varphi}_{22}+\widehat{\varphi}_{12}-\phi_0-\widehat{\varphi}_{11})}\right)\\
& +n_1e^{-j\widehat{\varphi}_{11}}-n_2e^{\,j(-\widehat{\varphi}_{22}+\widehat{\varphi}_{12}-\phi_0-\widehat{\varphi}_{11})}\Big],\\
y_2 = & \frac{1}{1-e^{-j2\phi_0}}\Big[s_2\left(e^{\,j(\varphi_{22}-\widehat{\varphi}_{22}+\widehat{\varphi}_{12}-\widehat{\varphi}_{12})}-e^{j(-2\phi_0+\varphi_{12}-\widehat{\varphi}_{12})}\right)\\
& +s_1\left(e^{\,j(-\phi_0+\varphi_{21}-\widehat{\varphi}_{22}+\widehat{\varphi}_{12}-\widehat{\varphi}_{12})}-e^{j(\varphi_{11}-\phi_0-\widehat{\varphi}_{12})}\right)\\
& +n_2e^{\,j(-\widehat{\varphi}_{22}+\widehat{\varphi}_{12}-\widehat{\varphi}_{12})}-n_1e^{j(-\phi_0-\widehat{\varphi}_{12})}\Big].
\end{aligned}\tag{16}$$

The above expressions can be simplified thanks to $(1-e^{-j2\phi_0})=2e^{j(-\phi_0+\pi/2)}\sin(\phi_0)$ and $(\varphi_{11}-\varphi_{21})=(\varphi_{22}-\varphi_{12})$ so deriving

$$\begin{aligned}
y_1 = & \frac{1}{1-e^{-j2\phi_0}}\Bigg[2\cdot s_1\cdot e^{j(-\phi_0+\pi/2)}\cdot e^{\,j\left(\varphi^e_{11}-\frac{\varphi^e_{22}}{2}+\frac{\varphi^e_{12}}{2}\right)}\cdot\sin\left(\phi_0-\frac{\Delta\phi^e_{R2}}{2}\right)\\
& +2\cdot s_2\cdot e^{j(-\phi_0+\pi/2)}\cdot e^{-j\Delta\phi_T}\cdot e^{\,j\left(-\varphi^e_{11}-\frac{\varphi^e_{22}}{2}+\frac{\varphi^e_{12}}{2}\right)}\cdot\sin\left(-\frac{\Delta\phi^e_{R2}}{2}\right)\\
& +n_1\cdot e^{-j\widehat{\varphi}_{11}}-n_2\cdot e^{j(-\widehat{\varphi}_{22}+\widehat{\varphi}_{12}-\phi_0-\widehat{\varphi}_{11})}\Bigg],\\
y_2 = & \frac{1}{1-e^{-j2\phi_0}}\Bigg[2\cdot s_2\cdot e^{j(-\phi_0+\pi/2)}\cdot e^{\,j\left(\frac{\varphi^e_{22}}{2}+\frac{\varphi^e_{12}}{2}\right)}\cdot\sin\left(\phi_0-\frac{\Delta\phi^e_{R2}}{2}\right)\\
& +2\cdot s_1\cdot e^{j(-\phi_0+\pi/2)}\cdot e^{-j\Delta\phi_T}\cdot e^{-j\left(\frac{\varphi^e_{22}}{2}+\frac{\varphi^e_{12}}{2}\right)}\cdot\sin\left(\frac{\Delta\phi^e_{R2}}{2}\right)\\
& +n_2\cdot e^{-j\widehat{\varphi}_{22}}-n_1\cdot e^{j(-\phi_0-\widehat{\varphi}_{12})}\Bigg].
\end{aligned}\tag{17}$$

It is interesting to observe that the phase noise estimation errors generate (I) an amplitude modulation proportional to $\sin\left(\phi_0-\frac{\Delta\phi^e_{R2}}{2}\right)$, (II) a phase modulation by the factors $e^{\,j\left(\varphi^e_{11}-\frac{\varphi^e_{22}}{2}+\frac{\varphi^e_{12}}{2}\right)}$ and $e^{\,j\left(\frac{\varphi^e_{22}}{2}+\frac{\varphi^e_{12}}{2}\right)}$ on the branches 1 and 2 respectively, (III) a residual interference from the cross path proportional to $\sin\left(\frac{\Delta\phi^e_{R2}}{2}\right)$. It is also worthy of consideration how this receiver operates asymmetrically on the recovered signals providing a benefit to the branch 2, due to the phase rotation by the factor $\Delta\widehat{\phi}_{R2}$ which involves the same estimation $\widehat{\varphi}_{12}$ used to correct the signal phase in the last stage of the receiver. This phase compensation, which cancels the common estimation errors, does not occur for the recovered signal on the branch 1 (it would occur if $\Delta\widehat{\phi}_{R1}=\widehat{\varphi}_{21}-\widehat{\varphi}_{11}$ were used on the branch 1 instead of $\Delta\widehat{\phi}_{R2}$ on the branch 2). This effect improves the mean squared error at the output of the branch 2.

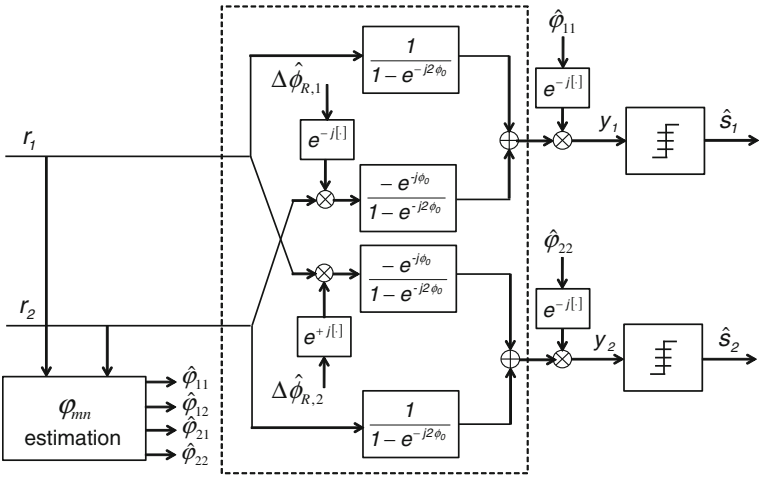

Fig. 4 Block diagram of symmetric receiver with $\Delta\phi_R$ correction

w.r.t. 1, even if the resulting gap turns out to be negligible as it will be shown in Sects. 4 and 5.

3.2.2 Symmetric Receiver with $\Delta\phi_R$ Correction

The asymmetric nature of the performance and the architecture of the previous receiver suggests a symmetric receiver structure, whose block diagram is shown in Fig. 4. Symmetry allows an easier and modular hardware implementation, especially if the estimation block is duplicated in two identical outdoor units forming the MIMO receiver. This architecture, according to authors' experience, should be especially advantageous if the distance between the two radio heads is taken into account. It is easy to derive the receiver block diagram in Fig. 4 rewriting the received signal vector $\mathbf{r}$ in (1) as

$$\mathbf{r} = \begin{bmatrix} 1 & e^{j(-\phi_0-\Delta\phi_{R2})} \\ e^{j(-\phi_0+\Delta\phi_{R1})} & 1 \end{bmatrix} \cdot \begin{bmatrix} s_1 e^{j\varphi_{11}} \\ s_2 e^{j\varphi_{22}} \end{bmatrix} + \begin{bmatrix} n_1 \\ n_2 \end{bmatrix}, \tag{18}$$

where $\Delta\phi_{R1} = \varphi_{21} - \varphi_{11} = \Delta\phi_{R2} = \varphi_{22} - \varphi_{12} = \Delta\phi_R$. Two stages can be observed in the receiver:

- A modified space equalization stage which operates a rotation on the cross branches (notice that this phase rotation is different from the rotation performed at stage 1 in Sect. 3.2.1).
- A direct phase noise cancelation on the two signals at the output of the equalizer by respectively $\widehat{\varphi}_{11}$ and $\widehat{\varphi}_{22}$.

Here the processing on the two branches is exactly the same, so exploiting the expedient of multiplying the received signals r_1 and r_2 respectively by the estimates $\Delta\widehat{\phi}_{R2}$ and $\Delta\widehat{\phi}_{R1}$, and operating the same beneficial compensation on estimated phases as already noticed for the branch 2 in Sect. 3.2.1. Here the equalizer matrix $\mathbf{W}_{\Delta\phi_R}$ is a modified version of (9),

$$\boldsymbol{W}_{\Delta\phi_R} = \frac{1}{1-e^{-j2\phi_0}} \begin{bmatrix} 1 & -e^{-j\phi_0} e^{-j\Delta\widehat{\phi}_{R1}} \\ -e^{-j\phi_0} e^{j\Delta\widehat{\phi}_{R2}} & 1 \end{bmatrix}. \tag{19}$$

So, from the definitions $\Delta\widehat{\phi}_{R1}$ and $\Delta\widehat{\phi}_{R2}$ (14) we have, after some manipulations similarly to (17),

$$
\begin{aligned}
y_1 = \frac{1}{1-e^{-j2\phi_0}} \Bigg[& 2 \cdot s_1 \cdot e^{j(-\phi_0+\pi/2)} \cdot e^{j\left(\frac{\varphi^e_{21}}{2}+\frac{\varphi^e_{11}}{2}\right)} \cdot \sin\left(\phi_0 + \frac{\Delta\phi^e_{R1}}{2}\right) \\
& + 2 \cdot s_2 \cdot e^{j(-\phi_0+\pi/2)} \cdot e^{j\Delta\phi_T} \cdot e^{-j\left(\frac{\varphi^e_{21}}{2}+\frac{\varphi^e_{11}}{2}\right)} \cdot \sin\left(-\frac{\Delta\phi^e_{R1}}{2}\right) \\
& + n_1 \cdot e^{-j\widehat{\varphi}_{11}} - n_2 \cdot e^{j(-\phi_0-\widehat{\varphi}_{21})} \Bigg], \\
y_2 = \frac{1}{1-e^{-j2\phi_0}} \Bigg[& 2 \cdot s_2 \cdot e^{j(-\phi_0+\pi/2)} \cdot e^{j\left(\frac{\varphi^e_{22}}{2}+\frac{\varphi^e_{12}}{2}\right)} \cdot \sin\left(\phi_0 - \frac{\Delta\phi^e_{R2}}{2}\right) \\
& + 2 \cdot s_1 \cdot e^{j(-\phi_0+\pi/2)} \cdot e^{-j\Delta\phi_T} \cdot e^{-j\left(\frac{\varphi^e_{22}}{2}+\frac{\varphi^e_{12}}{2}\right)} \cdot \sin\left(\frac{\Delta\phi^e_{R2}}{2}\right) \\
& - n_1 \cdot e^{j(-\phi_0-\widehat{\varphi}_{12})} + n_2 \cdot e^{-j\widehat{\varphi}_{22}} \Bigg].
\end{aligned}
\tag{20}
$$

As expected, we obtain a perfect symmetry between the two equations, with both the recovered signals y_1 and y_2 showing the same performance, in terms of residual phase noise and interference impairments, as for the branch 2 in the asymmetric receiver scheme.

3.2.3 Symmetric Space Equalization with $\Delta\phi_T$ Correction Stage

An alternative symmetric receiver, shown in Fig. 5, on the cross-branches of the equalizer uses the rotation angles $\Delta\widehat{\phi}_{T1} = \widehat{\varphi}_{12} - \widehat{\varphi}_{11}$ and $\Delta\widehat{\phi}_{T2} = \widehat{\varphi}_{22} - \widehat{\varphi}_{21}$, i.e. the estimates of the difference of the phase noises generated at the transmitter, instead of $\Delta\widehat{\phi}_{R1}$ and $\Delta\widehat{\phi}_{R2}$. Similarly to the derivation in Sect. 3.2.2, rewriting the received signal vector $\mathbf{r}$ in (1) as

$$
\mathbf{r} = \begin{bmatrix} e^{j\varphi_{11}} & e^{j\varphi_{11}} \cdot e^{j(-\phi_0+\Delta\phi_{T1})} \\ e^{j\varphi_{22}} \cdot e^{j(-\phi_0-\Delta\phi_{T2})} & e^{j\varphi_{22}} \end{bmatrix} \cdot \begin{bmatrix} s_1 \\ s_2 \end{bmatrix} + \begin{bmatrix} n_1 \\ n_2 \end{bmatrix},
\tag{21}
$$

with $\Delta\phi_{T1} = \varphi_{12} - \varphi_{11} = \Delta\phi_{T2} = \varphi_{22} - \varphi_{21} = \Delta\phi_T$, suggests a receiver with the two following stages:

- A direct phase noise cancelation on the received signals r_1 and r_2 by the estimates $\widehat{\varphi}_{11}$ and $\widehat{\varphi}_{22}$ respectively. This step substitutes the final correction step in the previous scheme.
- A space equalization stage with a rotation block on the cross branches, according to the matrix $\boldsymbol{W}_{\Delta\phi_T}$

$$
\boldsymbol{W}_{\Delta\phi_T} = \frac{1}{1-e^{-j2\phi_0}} \begin{bmatrix} 1 & -e^{-j\phi_0} e^{j\Delta\widehat{\phi}_{T2}} \\ -e^{-j\phi_0} e^{-j\Delta\widehat{\phi}_{T1}} & 1 \end{bmatrix}.
\tag{22}
$$

Output signals y_1 and y_2 can be easily derived as in previous sections and they show the same expressions as in (20), meaning that the two symmetric schemes in Figs. 4 and 5 are equivalent in terms of performance.

Note that the $\Delta\phi_R$ or $\Delta\phi_T$ correction in all the three receiver schemes plays the role of synchronization of the oscillators at the receiver or the transmitter side.

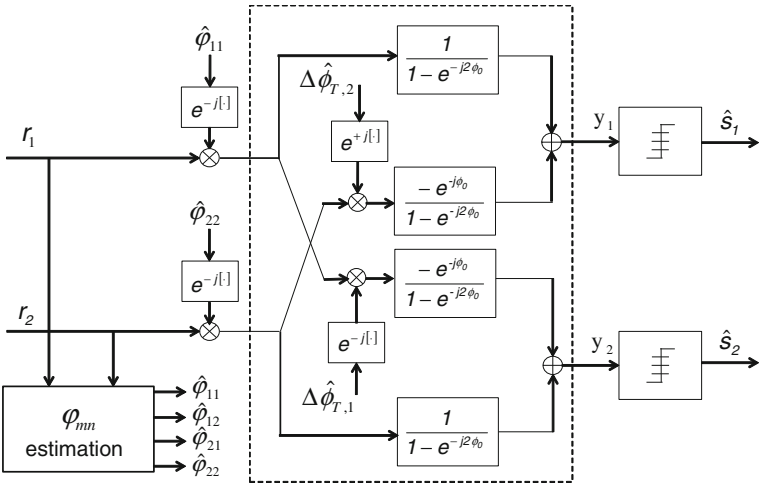

Fig. 5 Block diagram of symmetric receiver with $\Delta\phi_T$ correction

4 Analysis of Phase Noise Impact on the System

This section is devoted to the analytical derivations of the impact of the residual phase noise impairments on the system performance for the space equalization and phase noise suppression receiver structures described in Sect. 3.2. In addition we will consider the two extreme cases regarding the correlation between phase noise sources, i.e. coherent and non-coherent phase noise sources at the transmitter and receiver. The system performance is measured in terms of Noise-to-Signal Ratio NSR_m ($m = 1, 2$) on the two output branches

$$NSR_1 = \frac{E\left[|y_1 - s_1|^2\right]}{E\left[|s_1|^2\right]},$$
$$NSR_2 = \frac{E\left[|y_2 - s_2|^2\right]}{E\left[|s_2|^2\right]}. \tag{23}$$

Starting from the asymmetric receiver with $\Delta\phi_R$ correction (Fig. 3) we rewrite the output signals y_1 and y_2 (17) as

$$y_1 = \frac{1}{\sin(\phi_0)}\left[s_1 e^{j\beta_1}\sin(\phi_0 - \alpha) + s_2 e^{-j\,\Delta\phi_T} e^{j\delta_1}\sin(-\alpha)\right] + q_1,$$
$$y_2 = \frac{1}{\sin(\phi_0)}\left[s_2 e^{j\beta_2}\sin(\phi_0 - \alpha) + s_1 e^{-j\,\Delta\phi_T} e^{j\delta_2}\sin(\alpha)\right] + q_2, \tag{24}$$

where the parameters α, β_m and δ_m ($m = 1, 2$) are the following combinations of the residual phase estimation errors

$$\alpha = \frac{\varphi^e_{22} - \varphi^e_{12}}{2},\ \beta_1 = \varphi^e_{11} - \frac{\varphi^e_{22} - \varphi^e_{12}}{2},\ \delta_1 = -\varphi^e_{11} - \frac{\varphi^e_{22} - \varphi^e_{12}}{2},$$
$$\beta_2 = \frac{\varphi^e_{22} + \varphi^e_{12}}{2},\ \delta_2 = \frac{\varphi^e_{22} - \varphi^e_{12}}{2}, \tag{25}$$

and the filtered additive noise contributions q_1 and q_2 are

$$q_1 = \frac{2}{1 - e^{-j2\phi_0}} \left(n_1 e^{-j\widehat{\varphi}_{11}} - n_2 e^{j(-\phi_0 - \widehat{\varphi}_{21})} \right),$$
$$q_2 = \frac{2}{1 - e^{-j2\phi_0}} \left(n_2 e^{-j\widehat{\varphi}_{22}} - n_1 e^{j(-\phi_0 - \widehat{\varphi}_{12})} \right). \tag{26}$$

Except for a phase modulation factor $e^{-j\Delta\phi_T}$ on the cross path interference, (24) has the same expression of Eq. (16) in [7]: the residual phase noise degradation on the received signals generates a phase modulation by the factor $e^{j\beta_1}$ or $e^{j\beta_2}$, an amplitude modulation proportional to $\sin(\phi_0 - \alpha)$, and a residual interference from the cross path. In [7], where the real implementation of phase noise suppression methods is not considered, the residual phase noises were modeled as four i.i.d. white phase noise sources, two at the transmitter and two at the receiver with power ϵ^2 and a sufficiently small amplitude to validate in the analysis the approximations $\sin(\phi) \approx \phi$ and $\cos(\phi) \approx 1$.

Here the residual phase noise sources are the sum-processes estimation errors φ^e_{mn} at the output of the estimation process. In addition they are i.i.d. with small amplitude, zero mean $E[\varphi^e_{mn}] = 0$ and power $E[|\varphi^e_{mn}|^2] = \epsilon^2$ and hence we evaluate the *NSR* as in [7] and including the thermal noise contribution of the ZF equalization:

$$NSR_m = E[\beta_m^2] + E[\alpha^2] \frac{1 + \cos^2(\phi_0)}{\sin^2(\phi_0)} + \frac{\sigma_n^2}{2E_S \sin^2(\phi_0)}. \tag{27}$$

Equation (27) shows that the effect of $\alpha \neq 0$, i.e. not synchronized oscillators at the receiver, is amplified for small values of ϕ_0, regardless from the symbol energy E_S, and that the equalizer introduces a degradation on the input $SNR = E_S/N_0$ proportional to $sin^2(\phi_0)$ [7].

From (25) the values of $E\left[\alpha^2\right]$ and $E\left[\beta_m^2\right]$ turn out to be

$$E\left[\alpha^2\right] = \frac{\epsilon^2}{2}, E\left[\beta_1^2\right] = \frac{3\epsilon^2}{2}, E\left[\beta_2^2\right] = \frac{\epsilon^2}{2}, \tag{28}$$

giving rise to the asymmetric output performance $NSR_1 = NSR_2 + \epsilon^2$ already observed in Sect. 3.2.1.

Considering now the symmetric receivers, described in Sects. 3.2.2 and 3.2.3, it is easy to follow a similar procedure, achieving

$$E\left[\alpha^2\right] = \frac{\epsilon^2}{2}, E\left[\beta_1^2\right] = E\left[\beta_2^2\right] = \frac{\epsilon^2}{2}, \tag{29}$$

and confirming the symmetry between the two branches and the advantage provided by these types of architectures.

It is interesting to notice also that an improved estimate of $\Delta\phi_R$ ($\Delta\phi_T$), achieved by averaging $\Delta\widehat{\phi}_{R1}$ and $\Delta\widehat{\phi}_{R2}$ ($\Delta\widehat{\phi}_{T1}$ and $\Delta\widehat{\phi}_{T2}$), revealed no advantage in terms of *NSR* in all the receiver architectures if the appropriate $\Delta\phi_{Ri}$ ($\Delta\phi_{Ti}$) are applied as explained in Sect.3.2.2 and 3.2.3.

Finally, in case of perfectly synchronized oscillators at the receiver side $\rho_R = 1$, i.e. $\phi_1^{(R)} = \phi_2^{(R)} = \phi^{(R)}$, a simplified structure for the receiver should be considered. In fact, in this case the four phase noise sum-processes are equal two by two as

$$\varphi_{11} = \varphi_{21} = \phi_1^{(T)} + \phi^{(R)} = \varphi_1,$$
$$\varphi_{12} = \varphi_{22} = \phi_2^{(T)} + \phi^{(R)} = \varphi_2, \tag{30}$$

Table 1 Performance of receiver architectures in terms of amplitude and phase modulation degradation, measured as powers $E[\alpha^2]$, $\left[\beta_1^2\right]$ and $\left[\beta_2^2\right]$

Architecture	$\rho_R = 0, \rho_T = 0$	$\rho_R = 1, \rho_T = 0$	$\rho_R = 0, \rho_T = 1$
Asymmetric	$E\left[\alpha^2\right] = \epsilon^2/2$		
$\Delta\phi_R$ correction	$E\left[\beta_1^2\right] = 3\epsilon^2/2$		
	$E\left[\beta_2^2\right] = \epsilon^2/2$		
Symmetric	$E\left[\alpha^2\right] = \epsilon^2/2$	$E\left[\alpha^2\right] = 0$	
$\Delta\phi_R$ correction	$E\left[\beta_1^2\right] = E\left[\beta_2^2\right] = \epsilon^2/2$	$E\left[\beta_1^2\right] = E\left[\beta_2^2\right] = \epsilon^2/2$	
Symmetric	$E\left[\alpha^2\right] = \epsilon^2/2$		$E\left[\alpha^2\right] = \epsilon^2/2$
$\Delta\phi_T$ correction	$E\left[\beta_1^2\right] = E\left[\beta_2^2\right] = \epsilon^2/2$		$E\left[\beta_1^2\right] = E\left[\beta_2^2\right] = \epsilon^2/4$

and they should be estimated jointly to avoid the generation of four independent errors, i.e. by $\widehat{\varphi}_1 = \frac{\widehat{\varphi}_{11}+\widehat{\varphi}_{21}}{2}$ and $\widehat{\varphi}_2 = \frac{\widehat{\varphi}_{12}+\widehat{\varphi}_{22}}{2}$ resulting in estimation error powers $E\left[\varphi_1^2\right] = E\left[\varphi_2^2\right] = \epsilon^2/2$. In this case, in the block diagram of Fig. 4, the first phase correction stage is no more necessary since $\Delta\widehat{\varphi}_{R1} = \Delta\widehat{\varphi}_{R2}$ is forced to 0 (note that, on the contrary, the simplification cannot be introduced in the receiver scheme of Fig. 5) and the signals y_1 and y_2 are easily updated as

$$
\begin{aligned}
y_1 &= e^{-j\varphi_1^e} \cdot s_1 + \frac{e^{-j\widehat{\varphi}_1}}{1 - e^{-j2\phi_0}} \left(n_1 - n_2 \cdot e^{-j\phi_0}\right), \\
y_2 &= e^{-j\varphi_2^e} \cdot s_2 + \frac{e^{-j\widehat{\varphi}_2}}{1 - e^{-j2\phi_0}} \left(n_2 - n_1 \cdot e^{-j\phi_0}\right).
\end{aligned} \tag{31}
$$

Equation (31) highlights the advantage of a synchronization device between the oscillators at the receiver antennas as $\alpha = 0$ means no amplitude modulation in (28), (29) while the phase modulation does not change $\left(E\left[\beta_1^2\right] = E\left[\beta_2^2\right] = E\left[\left(\varphi_1^e\right)^2\right] = E\left[\left(\varphi_2^e\right)^2\right] = \epsilon^2/2\right)$.

In a dual way, in case of perfectly synchronized oscillators at the transmitter side ($\rho_T = 1$), the condition $\phi_1^{(T)} = \phi_2^{(T)} = \phi^{(T)}$ provides, similarly to (30), two phase noise sum-processes

$$
\begin{aligned}
\varphi_{11} = \varphi_{12} &= \phi_1^{(R)} + \phi^{(T)} = \varphi_1, \\
\varphi_{21} = \varphi_{22} &= \phi_2^{(R)} + \phi^{(T)} = \varphi_2,
\end{aligned} \tag{32}
$$

showing the same architectural advantage explained above for the correlated oscillators at the receiver, if applied here to the block diagram of Fig.5 where $\Delta\widehat{\phi}_{T1}$ and $\Delta\widehat{\phi}_{T2}$ are forced to 0. A slighter performance improvement is expected, w.r.t. the improvement provided by $\rho_R = 1$, as $E\left[\alpha^2\right]$ decreases to $\epsilon^2/4$ but the amplitude modulation remains. Negligible improvement are expected also by the smaller phase modulation effect, $E\left[\beta_1^2\right] = E\left[\beta_2^2\right] = E\left[\frac{\varphi_1^2}{2} + \frac{\varphi_2^2}{2}\right] = \epsilon^2/4$, and by the simplification of the factor $e^{-j\Delta_T} = 1$ in (20).

Table 1 summarizes the different receiver architectures performance in terms of amplitude and phase modulation impact measured as powers $E\left[\alpha^2\right]$, $\left[\beta_1^2\right]$, $\left[\beta_2^2\right]$.

5 Numerical Results

In this Section we present the numerical results obtained by the analysis and the simulations of a LoS-MIMO (2×2) system whose receiver is implemented according to the phase noise estimation methods and suppression schemes described in Sect. 3. The numerical results are divided in two groups for presenting (I) the performance comparison among the different phase estimation methods in terms of mean squared estimation error (Sect. 5.1) and (II) the overall system performance in terms of the Symbol Error Rate (SER) or the output Signal-to-Noise ratio $SNR_{OUT} = NSR^{-1}$ (Sect. 5.2). In the plots, the input ratio $SNR = E_S/N_0$ is measured at the receiver side (so different SNRs might correspond to different link distances) while the phase noise level introduced by the oscillators is returned by means of the ratio $NSR_{TOT} = \varepsilon_{TOT}^2/E_S$, i.e. the ratio between the total phase noise power at one of the four sources and the average symbol energy. The reference mask of the phase noise power spectral density is $[-55, -75, -95]$ dBc/Hz at $[10^3, 10^4, 10^5]$ Hz. The symbol rate of the signal is equal to 10^7 symbols/s. In order to clarify the impact of the residual phase noise on the system, we provide also, as a reference, the factor $\Delta_{PHN} = \epsilon^2/N_0$, i.e. the ratio between the residual phase noise and the thermal noise powers; this factor was used in [7] for extrapolating the link distances achievable by the system. All the results refer to transmission of 64-QAM data symbols and binary pilot symbols with symbol energy E_S .

5.1 Phase Noise Estimation Performance

Performance of different phase noise estimators is compared for different values of *SNR*, NSR_{TOT} and pilot period P in order to understand the most appropriate design lines for the system under investigation. Figures 6 and 7 report the average estimation error power

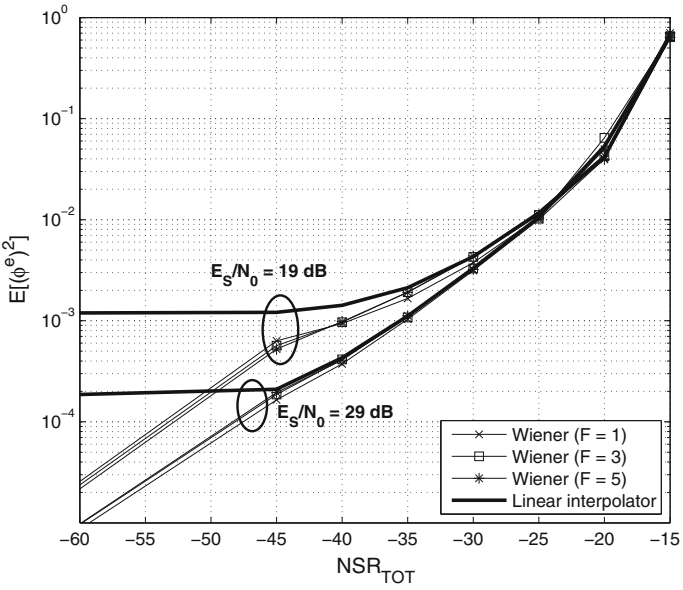

Fig. 6 Mean squared estimation error as a function of NSR_{TOT} at two different *SNR* values and for different phase noise estimators

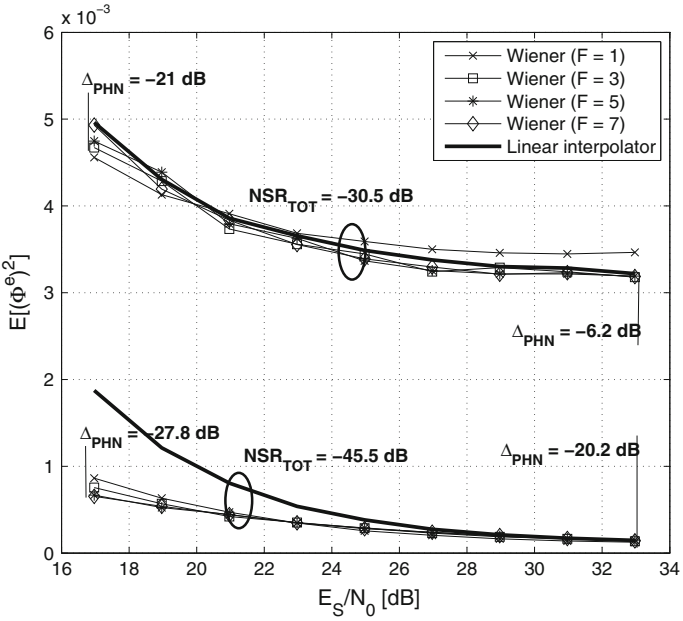

Fig. 7 Mean squared estimation error as a function of *SNR* at two different NSR_{TOT} values and for different phase noise estimators. Some measured values of the Δ_{PHN} parameter are reported for reference

$E\left[\left|(\phi^e)^2\right|\right] = \frac{1}{4}\sum_{m,n=1,2} E\left[\left|\varphi^e_{mn}\right|^2\right]$ as a function of the total phase noise power ϵ^2_{TOT} fixed the *SNR*, and viceversa, as a function of the *SNR* fixed ϵ^2_{TOT}. The numerical findings show that the Wiener filter outperforms the linear interpolator for low values of NSR_{TOT} and low values of *SNR* with negligible improvement for different lengths $F = 1, 3, \ldots, 7$. The linear interpolator becomes the most attractive design choice for its simplicity at medium-high NSR_{TOT} (medium high phase noise levels) and medium-high *SNR*, showing a performance comparable with the longest simulated Wiener $F = 5$. In Fig. 7 the measured values of the Δ_{PHN} parameter, used in [7] for extrapolating the link distances achievable by the system, are reported for reference: in the high *SNR* region, supposed to be the common working condition for LoS-MIMO multiplexing, the operating range of Δ_{PHN} ($\Delta_{PHN} < -13$ dB in Figs.10 and 11, [7]) can be achieved for $NSR_{TOT} = -45.5$ dB but not for $NSR_{TOT} = -30.5$ dB. Then Fig. 8 can be used for evaluating the impact of the pilots period in the simulated phase noise statistics; we can observe, again, similar performance between the linear interpolator and the Wiener's filter with any length F. In addition, it can be observed how the low frequency components of the phase noise model make the final performance not strongly dependent from P, either at low or high *SNR* values. The plots of the next section will assume the two best estimators with $P = 10$, i.e. the linear interpolator and the Wiener's filter with $F = 5$.

5.2 Phase Noise Suppression and System Performance

The final signal-to-noise ratio SNR_{OUT}, at the output of the two branches, is affected not only by the phase noise estimation process but also by the channel parameter ϕ_0 and by the suppression and equalization architecture, as discussed in Sect. 3. Fixed the channel parameter $\phi_0 = \pi/2$, for $\rho_R = \rho_T = 0$, Fig. 9 shows SNR_{OUT} versus NSR_{TOT}, confirming that

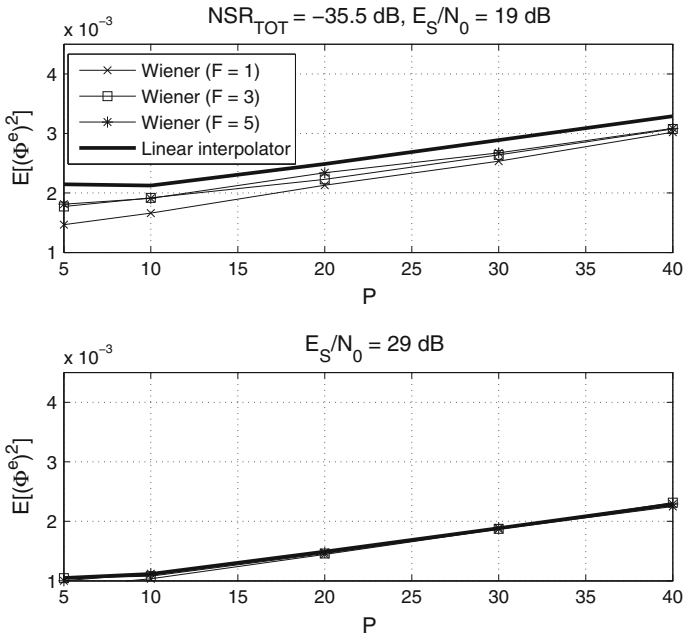

Fig. 8 Mean squared estimation error as a function of the pilot period P at different SNR and NSR_{TOT} values

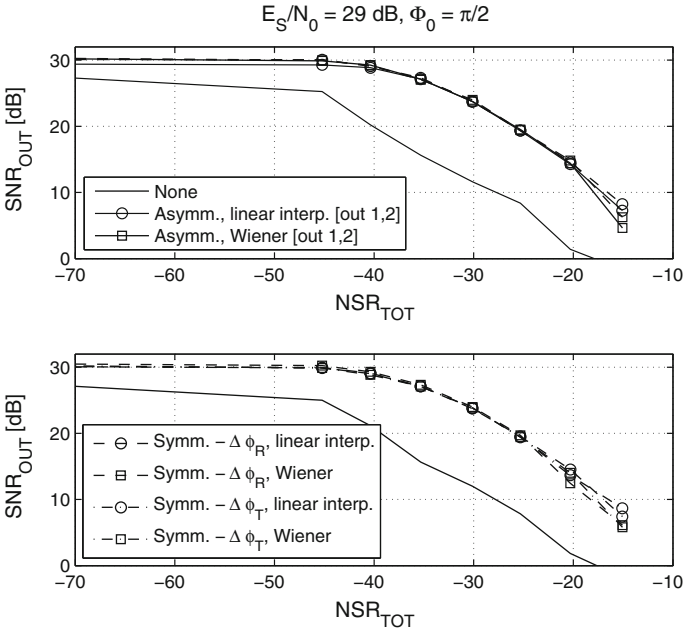

Fig. 9 Output SNR as a function of NSR_{TOT} at $SNR = 29\,\text{dB}$ for different phase noise suppression and equalization architectures. The *top figure* reports SNR_{OUT} at the output of the two branches separately (*continuous and dashed lines*)

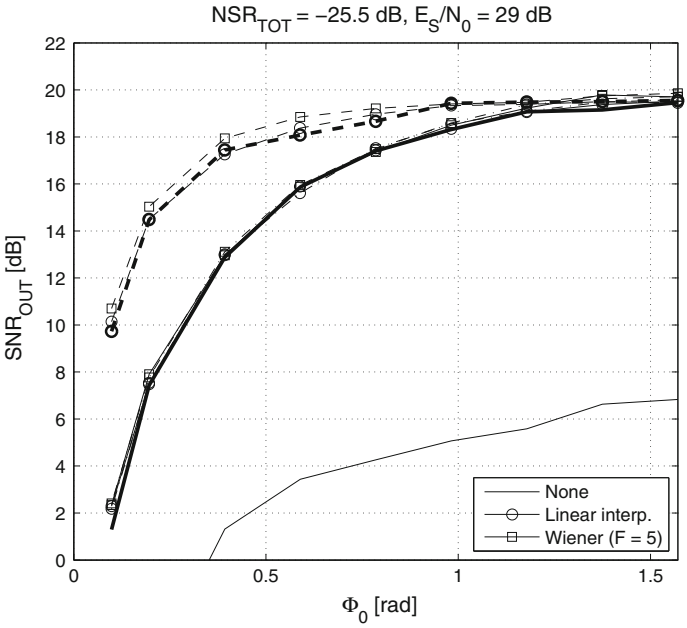

Fig. 10 Output SNR as a function of ϕ_0 at $NSR_{TOT} = -25.5\,\text{dB}$ and $SNR = 29\,\text{dB}$ for the symmetric receiver with $\Delta\phi_R$ correction (other architectures give equivalent results). *Continuous*, *normal lines* refer to non-coherent phase noise sources ($\rho_T = \rho_R = 0$), *dashed lines* to $\rho_T = 0$ and $\rho_R = 1$ and *dash-dotted lines* to $\rho_T = 1$ and $\rho_R = 0$. *Bold lines* (*continuous* for non coherent and *dashed* for coherent phase noise sources) are obtained by means of the analysis presented in Sect. 4

- in typical system working regions, the linear interpolator and the Wiener's filter with $F = 5$ have similar performance,
- all the suppression and equalization architectures have very similar performance too,
- the asymmetric receiver scheme with $\Delta\phi_R$ correction has a slightly lower performance on one of the the two branches as predicted by the analysis even if practically negligible (Fig. 9, top).

Then the impact of other two parameters of the system, i.e. the channel phase ϕ_0 and the correlation degree among the phase noise sources, are shown in Fig. 10. As predicted by the analysis, the channel cross angle ϕ_0 has a relevant impact on system performance (27), especially for $\rho_R = 0$. The beneficial role of phase noise correlation at the receiver ($\rho_R > 0$ till to 1) is to enhance performance while simplifying the receiver architecture based on $\Delta\phi_R$ correction, as underlined in the analysis. It is also verified that phase noise correlation at the transmitter ($\rho_T > 0$ till to 1) gives negligible performance improvement. We observe how the analysis performed according to the procedure presented in Sect. 4 returns values which fit well the simulated results, for either $\rho_R = 0$ or $\rho_R = 1$.

Finally, Figs. 11 and 12 report the results for output SER versus input SNR respectively for two values of channel angle, $\phi_0 = \pi/2$ that guarantees the full-rank channel matrix, and $\phi_0 = \pi/8$, i.e. the operating value for practical systems that require to limit the distance between the antennas. For a fair comparison between PA and non PA transmission systems the results take into account that, for pilot pattern transmission, the effective energy per data symbols is decreased by the factor $(P-2)/P$ (about 1 dB) w.r.t. the symbol energy E_S experienced by the system without pilots. This energy loss is the reason for the Wiener filter

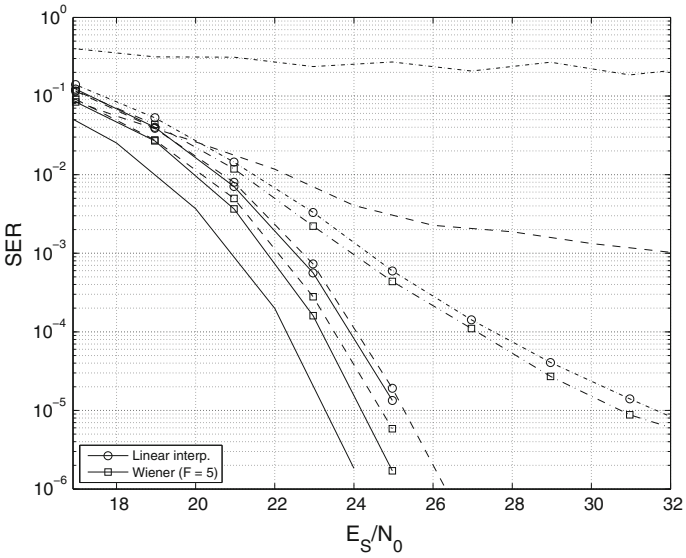

Fig. 11 Output SER as a function of *SNR* at $\phi_0 = \pi/2$ and $NSR_{TOT} = 0$ (*continuous lines*), $NSR_{TOT} = -43\,\text{dB}$ (*dashed lines*), $NSR_{TOT} = -33\,\text{dB}$ (*dash-dotted lines*). The receivers are based on the symmetric scheme with $\Delta\phi_R$ correction (other architectures give equivalent results)

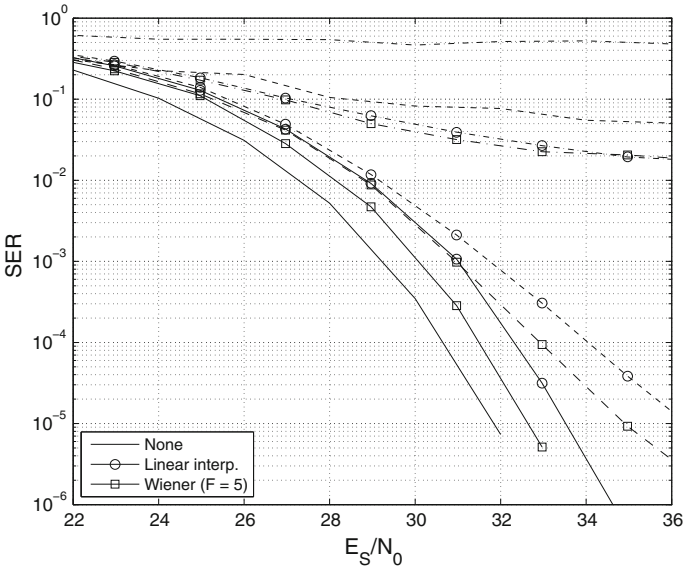

Fig. 12 Output SER as a function of *SNR* at $\phi_0 = \pi/8$ and $NSR_{TOT} = 0$ (*continuous lines*), $NSR_{TOT} = -43\,\text{dB}$ (*dashed lines*), $NSR_{TOT} = -33\,\text{dB}$ (*dash-dotted lines*). The receivers are based on the symmetric scheme with $\Delta\phi_R$ correction (other architectures give equivalent results)

degradation w.r.t. no pilot transmission for very low levels of phase noise. The results confirm that a difference between the Wiener filter and the linear interpolator can be appreciated at low values of phase noise power ($NSR_{TOT} < -33$ dB) and particularly for lower values of

the channel angle ϕ_0 (e.g. $\phi_0 = \pi/8$ in Fig. 12) where the difference achieves about 1 dB for the value $NSR_{TOT} = -43$ dB of interest for practical implementation ([7]).

6 Conclusions

We have highlighted the impact of the short-term random fluctuations of phase noise in the Los-MIMO (2×2) system specifically intended for practical PtP high throughput backhauling microwave links, for which the high SNR region and low antennas separations are the operating conditions. We presented and compared three different receiver architectures for phase noise suppression and two linear PA phase noise estimation methods, i.e. the simple linear interpolator and the Wiener filter with different lengths. By analysis and numerical simulations, we showed that (I) a pilot transmission with period $P = 10$ and a simple linear interpolator track efficiently the phase noise low frequency components, (II) a symmetric receiver with $\Delta\phi_R$ correction is an advantageous solution from a practical point of view, (III) a single oscillator reference at the two receiver branches would provide substantial performance improvement, not achievable through the synchronization of the oscillators at the transmitter. The analytical and numerical results, which proved the feasibility and efficiency of phase noise suppression circuits in presence of multiple phase noise sources, can be extended to other multiplexing strategies for microwave link, including dual polarization systems.

7 Appendix: A Wiener filter for the 2 × 2 LoS-MIMO

The variables (12) are observed during F pilot periods, each one of length P symbols, generating $(F+1)$ observables. These variables are collected in the column vector $\boldsymbol{\eta}_{lP}$, where lP is the current pilot time instant. Observations span from $(lP - L)$ to $(lP - L + FP)$ with $L = \lfloor F/2 \rfloor P$. From vector $\boldsymbol{\eta}_{lP}$, of length $4(F+1)$,

$$\boldsymbol{\eta}_{lP} = \begin{bmatrix} \eta_{11;lP-L} \\ \vdots \\ \eta_{11;lP-L+FP} \\ \hline \eta_{21;lP-L} \\ \vdots \\ \eta_{21;lP-L+FP} \\ \hline \eta_{12;lP-L} \\ \vdots \\ \eta_{12;lP-L+FP} \\ \hline \eta_{22;lP-L} \\ \vdots \\ \eta_{22;lP-L+FP} \end{bmatrix} = \begin{bmatrix} \boldsymbol{\eta}_{11;lP} \\ \hline \boldsymbol{\eta}_{21;lP} \\ \hline \boldsymbol{\eta}_{12;lP} \\ \hline \boldsymbol{\eta}_{22;lP} \end{bmatrix}, \tag{33}$$

the cross covariance matrix $\boldsymbol{C}_{\eta\eta}$ with dimension $4(F+1)\times 4(F+1)$ is computed as

$$\boldsymbol{C}_{\eta\eta} = E_l\left[\boldsymbol{\eta}_{lP}\boldsymbol{\eta}_{lP}^T\right]. \tag{34}$$

Its generic element in position $(i,\, j)$ can be expressed as

$$\boldsymbol{C}_{\eta\eta}(i,\, j) = E_l\left[\eta_{m_1n_1;lP}\cdot\eta_{m_2n_2;lP+\Delta}\right] = r_{m_1n_1;m_2n_2}(\Delta), \tag{35}$$

with $m_1, n_1, m_2, n_2 = 1, 2$, $\Delta\in[-FP : P : FP]$, $i = [(F+1)(m_1-1+(n_1-1)2(F+1))+|\Delta/P|+1]$ and $j = [(F+1)(m_2-1+(n_2-1)2(F+1))+|\Delta/P|+1]$, and where the cross correlation $r_{m_1n_1;m_2n_2}(\Delta)$, assuming uncorrelated phase noise processes between transmitter and receiver, can be expressed as

$$r_{m_1n_1;m_2n_2}(\Delta) = r^{(R)}_{m_1m_2}(\Delta) + r^{(T)}_{n_1n_2}(\Delta) + \frac{\sigma_n^2}{2}\delta(m_1-m_2)\delta(n_1-n_2)\delta(\Delta), \tag{36}$$

with $r^{(R)}_{m_1m_2}$ and $r^{(T)}_{n_1n_2}$ the correlations between phase noise processes respectively at the two receivers and at the two transmitters. Only for $m_1 = m_2$, $n_1 = n_2$ and $\Delta = 0$ the noise term is present (additive noise contributions are assumed uncorrelated).

To estimate the phase noise processes $\widehat{\varphi}_{mn;lP+i}$, where $i = 2, 3, \cdots, (P-1)$ is the interpolating symbol instant, four filter coefficients vectors of length $(F+1)$, i.e. a total of $4(F+1)$ coefficients, are computed according to

$$\mathbf{w}_{mn;i} = \boldsymbol{C}^{-1}_{\eta\eta}\mathbf{c}_{\eta\varphi_{mn;i}}, \tag{37}$$

where the vector $\mathbf{c}_{\eta\varphi_{mn;lP+i}}$ contains the correlations $E[\boldsymbol{\eta}_{lP}\cdot\varphi_{mn;lP+i}]$, i.e.

$$\mathbf{c}_{\eta\varphi_{mn;i}} = \begin{bmatrix} E_l[\eta_{11;lP-L}\cdot\varphi_{mn;lP+i}] \\ E_l[\eta_{11;lP-L+P}\cdot\varphi_{mn;lP+i}] \\ \vdots \\ E_l[\eta_{11;lP-L+FP}\cdot\varphi_{mn;lP+i}] \\ ---------- \\ E_l[\eta_{21;lP-L}\cdot\varphi_{mn;lP+i}] \\ E_l[\eta_{21;lP-L+P}\cdot\varphi_{mn;lP+i}] \\ \vdots \\ E_l[\eta_{21;lP-L+FP}\cdot\varphi_{mn;lP+i}] \\ ---------- \\ E_l[\eta_{12;lP-L}\cdot\varphi_{mn;lP+i}] \\ E_l[\eta_{12;lP-L+P}\cdot\varphi_{mn;lP+i}] \\ \vdots \\ E_l[\eta_{12;lP-L+FP}\cdot\varphi_{lP+i}] \\ ---------- \\ E_l[\eta_{22;lP-L}\cdot\varphi_{mn;lP+i}] \\ E_l[\eta_{22;lP-L+P}\cdot\varphi_{mn;lP+i}] \\ \vdots \\ E_l[\eta_{22;lP-L+FP}\cdot\varphi_{mn;lP+i}] \end{bmatrix}. \tag{38}$$

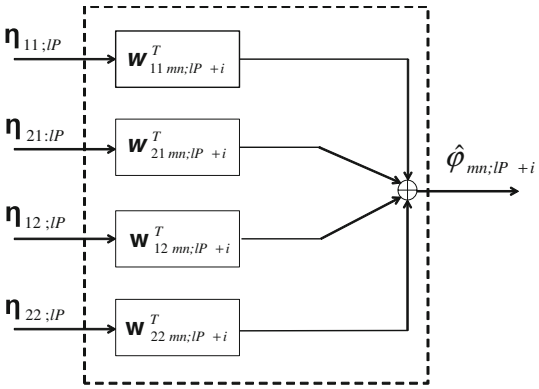

Fig. 13 The four-dimensional Wiener filter block diagram

The four-dimensional Wiener coefficients vectors $\mathbf{w}_{mn;i}$, i.e.

$$\mathbf{w}_{mn;i} = \begin{bmatrix} w_{11mn;i;1} \\ \vdots \\ w_{11mn;i;F+1} \\ \hline w_{21mn;i;1} \\ \vdots \\ w_{21mn;i;F+1} \\ \hline w_{12mn;i;1} \\ \vdots \\ w_{12mn;i;F+1} \\ \hline w_{22mn;i;1} \\ \vdots \\ w_{22mn;i;F+1} \end{bmatrix} = \begin{bmatrix} \mathbf{w}_{11mn;i} \\ \hline \mathbf{w}_{21mn;i} \\ \hline \mathbf{w}_{12mn;i} \\ \hline \mathbf{w}_{22mn;i} \end{bmatrix}; \tag{39}$$

are then used to estimate the phase noise process as sketched in Fig. 13:

$$\widehat{\varphi}_{mn;lP+i} = \mathbf{w}_{mn;i}^{T} \boldsymbol{\eta}_{lP}. \tag{40}$$

Finally, assuming i.i.d. estimation error processes w.r.t. the period l and the indexes (m, n), the mean squared estimation error $E[(\varphi^e)^2]$ is defined as

$$E\left[\left(\varphi^e\right)^2\right] = \frac{1}{4(P-2)} trace\left(E_l\left[\left(\widehat{\boldsymbol{\varphi}}_{lP} - \boldsymbol{\varphi}_{lP}\right)\left(\widehat{\boldsymbol{\varphi}}_{lP} - \boldsymbol{\varphi}_{lP}\right)^T\right]\right), \tag{41}$$

where the sum-processes vectors $\boldsymbol{\varphi}_{lP}$ and $\widehat{\boldsymbol{\varphi}}_{lP}$ have length $4(P-2)$.

References

1. Coldrey, M., Koorapaty, H., Berg, J., Gebretensae, Z., Hansryd, J., Derneryd, A., & Falahati, S. (2012). Small-cell wireless backhauling: A non-line-of-sight approach for point-to-point microwave links. In *Proceedings of 2012 IEEE Vehicular Technology Conference-Fall 2012* (pp. 1–5).

2. Hansryd, J., & Edstam, J. (2011). Microwave capacity evolution. *Ericsson Review*, (1), 22–27.
3. Tipmongkolsilp, O., Zaghloul, S., & Jukan, S. (2011). The evolution of cellular backhaul technologies: Current issues and future trends. *IEEE Communications Surveys and Tutorials*, *13*(1), 97–113.
4. Driessen, P. F., & Foschini, G. J. (1999). On the capacity formula for multiple input-multiple output wireless channels: A geometric interpretation. *IEEE Transactions on Communications*, *47*(2), 173–176.
5. Bohagen, F., Orten, P., & Oien, G. E. (2007). Design of optimal high-rank line-of-sight MIMO channels. *IEEE Transactions Wireless Communications*, *6*(4), 1420–1425.
6. Calabrò, S., Lankl, B., & Sebald, G. (2004). Multiple co-polar co-channel point-to-point transmission. *AEU International Journal of Electronics and Communications*, *58*(1), 51–57.
7. Reggiani, L., Baccetti, B., & Dossi, L. (2013). The role of adaptivity in MIMO line-of-sight systems for high capacity backhauling. *Wireless Personal Communications*, *74*, 373–389.
8. Durisi, G., Tarable, A., Camarda, C., Devassy, R., & Montorsi, G. (2014). Capacity bounds for MIMO microwave backhaul links affected by phase noise. *IEEE Transactions on Communications*, *62*(3), 920–929.
9. Hadaschik, N., Dörpinghaus, M., Senst, A., Harmjanz, O., Käufer, U., Ascheid, G., et al. (2005). Improving MIMO phase noise estimation by exploiting spatial correlations. In *IEEE International Conference on ICASSP*.
10. Proakis, J. G. (1995). *Digital communications* (3rd ed.). New York: McGraw-Hill.
11. Simon, V., Senst, A., Speth, M., & Meyr, H. (2001). Phase noise estimation via adapted interpolation. *IEEE GLOBECOM'01*, *6*, 3297–3301.